Materials Process and Applications of Single Grain (RE)-Ba-Cu-O Bulk High-temperature Superconductors

Beizhan Li, Difan Zhou, Kun Xu, Shogo Hara, Keita Tsuzuki, Motohiro Miki, Brice Felder, Zigang Deng and Mitsuru Izumi*

Laboratory of Applied Physics, Department of Marine Electronics and Mechanical Engineering, Tokyo University of Marine Science and Technology (TUMSAT), 2-1-6, Etchu-jima, Koto-ku, Tokyo 135-8533, Japan
*E-mail: izumi@kaiyodai.ac.jp

Abstract **- This paper reviews recent advances in the melt process of (RE)-Ba-Cu-O [(RE)BCO, where RE represents a rare earth element] single grain high-temperature superconductors (HTS), bulks and its applications. The efforts on the improvement of the magnetic flux pinning with employing the top-seeded melt-growth process technique and using a seeded infiltration and growth process are discussed. Which including various chemical doping strategies and controlled pushing effect based on the peritectic reaction of (RE)BCO. The typical experiment results, such as the largest single domain bulk, the clear TEM observations and the significant critical current density, are summarized together with the magnetization techniques. Finally, we highlight the recent prominent progress of HTS bulk applications, including Maglev, flywheel, power device, magnetic drug delivery system and magnetic resonance devices.**

Preprint of plenary SCC paper submitted to *Physica C* (should be cited accordingly)
Submitted to ESNF November 30, 2011; accepted Dec. 6, 2011. Reference No. CR24; Category 3.

Keywords **– rare earth, cuprate, high-temperature superconductor, HTS, bulk superconductor, melt growth process, flux pinning, MAGLEV, MRI, Flywheel, Motor**

I. INTRODUCTION

Following the discovery of $YBa_2Cu_3O_{7-\delta}$[1], $(RE)Ba_2Cu_3O_{7-\delta}$, *i.e.*, (RE)BCO or RE-123 (RE = rare earth element or Y) bulk high-temperature superconductors (HTS) have attracted the worldwide study for their ability to trap large magnetic flux density of 17 T at 29 K [2] and 3 T at 77 K [3]. Those trapped fields are obviously higher than those of conventional permanent magnets and can be potentially used in a wide range of

sustainable engineering applications. Many prototype applications, such as fault current limiters, motors and generators, flywheel batteries, maglev and magnetic separation systems, have been designed [4-6]. For those applications, a very important parameter is the critical current density J_c, which determines the maximum electric current that is flowing without energy dissipation. However, typical values of J_c for bulk single grain materials are nearly two orders of magnitude lower than those achieved in thin-films or coated conductors. Due to short coherence lengths of HTS, which are 2-4 nm for YBCO below 77 K, various nano-sized structural disorder sources such as inclusions can be effective pinning centers. They prevent thermally activated giant flux motion, thereby resulting in large super-current and a high irreversibility field [6-8]. Nevertheless, it is not an easy task to implant the nano-sized pinning centers in the bulk. To improve J_c *via* material processing, including the control of crystal chemistry, melt growth, flux pinning, *etc*., is still a challenging task. Previous review articles on this topic are available in [9-17].

We briefly describe the recent progress, discuss the characterization of their microstructure and superconducting properties, and outline the prominent and emerging applications that incorporate bulk (RE)BCO materials.

II. DEVELOPMENT OF MELT TEXTURED (RE)BCO BULK SUPERCONDUCTORS

The trapped field $B_T \propto J_c \times R$, where R is the radius of the single domain, and J_c are approximately proportional to the interface area between the matrix and inclusions [16, 18]. Hence, introducing nano-sized defects and attaining large grain size are effective ways to get large B_T. For the improvement of J_c, one of the techniques is the addition of second phase particles into the superconducting matrix. To obtain large single grains, the most common method so far is to use the top seeded melt texture (TSMG) technique. A B_T near 10 T may be possible at 77 K if proper chemical pinning centers are created [19].

A. Melt Processing Techniques

Since the initiation of melt processing, significant progress has been achieved in the

development of melt texturing methods. Early stage explorations are found in ref. [20]. Nowadays, two kinds of melt processes are adopted based on the peritectic reaction of (RE)BCO: one is TSMG technique, the other is the infiltration and growth (IG) process. Correspondingly, the seeding technique has been developed to allow the so-called batch bulk process and controlled multi-domain bulk growth.

The TSMG Technique

The TSMG technique has been developed for the fabrication of large grain (RE)BCO bulk objects above the peritectic temperature T_p. In this reaction, solid (RE)BCO decomposes to form solid RE-211 and BaCuO-based liquid. A single grain is formed by cooling a molten (RE)BCO sample slowly through T_p. The process is as follows. The starting materials of (RE)BCO, RE-211, Ag_2O, Pt or CeO_2, *etc*., are thoroughly mixed. The mixture is uniaxially pressed into a pellet. Generally, the Y-stabilized ZrO_2 rods are used to support the pellet. A seed is placed on the top surface of the pre-sintered pellet (hot seeding method) or placed there at room temperature before melt processing (cold seeding method) to nucleate the growth of a single grain. The arrangement is then melt grown in a reduced oxygen partial pressure (oxygen controlled melt growth process, OCMG).

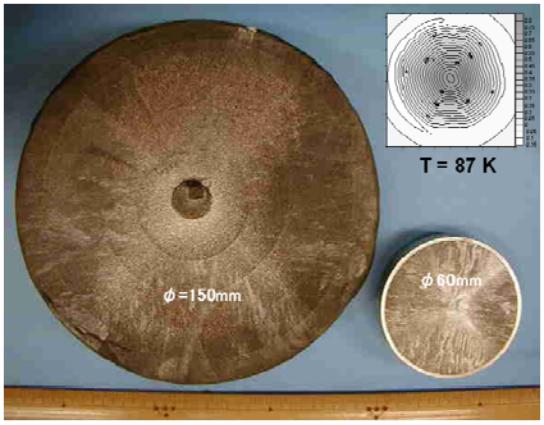

Fig. 1. Single domain bulk disks fabricated by employing the TSMG technique. The large disk has a diameter of 150 mm, the small one has a diameter of 60 mm. Inset illustrates the flux distributions in the large disk (courtesy of Hidekazu Teshima and Mitsuru Morita, Nippon Steel Corporation).

As the ionic radius of all RE^{3+} is close to Ba^{2+}, the $RE_{1+x}Ba_{2-x}Cu_3O_y$ solid solutions may form during melt process. The OCMG process can suppress the solid solution formation and thus increase T_c [21]. However, the OCMG process takes longer time and

involves higher cost than the air process. Therefore, the air process is preferentially adopted, especially for Gd-123. With adding Ba-rich compounds and employing Ar-post annealing (ArPA), the (RE)BCO superconductors are fabricated with high quality. Single-domain disks fabricated by optimized TSMG technique have been reported with diameters up to 140 mm [22-24]. A recent result (Nippon Steel Corporation, Japan) shows a diameter of 150 mm with a homogeneous flux distribution and a trapped flux density of over 0.8 T at 87 K, as shown in Figure 1. The TSMG technique has the disadvantage of easy coarsening, large shrinkage and liquid outflow. Macroscopic cracks and pores are also easy to form in the melt growth. The chemical composition of the final product is generally inhomogeneous.

The Seeded Infiltration and Growth (IG) Process

The IG process involves the infiltration of liquid phases into a pellet of RE-211 with subsequent reacting to form (RE)BCO below T_p. The IG process allows near arbitrary shape fabrication with negligible shrinkage and distortion [24, 25] of, *e.g.*, hollow cylinders [26], superconducting foams [27] and fabrics [28, 29]. The major advantage of the IG process compared to the TSMG process is the ability to provide fine-sized spherical RE-211 precipitates in the (RE)BCO matrix, even without addition of compounds such as Pt and CeO_2 [30-32]. It makes the IG process attractive. With a modified IG process, the value of J_c is up to 230 kA/cm^2 under zero-field and 10 kA/cm^2 up to 7 T at 77 K in YBCO [33]. However, the IG process has the disadvantage that the uniformity of microstructure and J_c is uncertain [31].

Seed Techniques

For both TSMG and IG process, a choice of the seed crystal is an important factor. It should have the lattice parameters close to those of (RE)BCO and remain stable during the whole melt process. As Nd-123 has the highest melting point (1068 ˚C) in the RE-123 family, Nd-123 crystals are usually employed as seeds for growth of other (RE)BCO bulk superconductors [14]. However, because the T_p of Nd-123 is not high enough, the kind of species which could be seeded in the (RE)BCO are limited [34]. The Mg-doped (> 0.5 wt.%) Nd-123 has the T_p by 20 ˚C higher than the T_p of pure Nd-123 [35]. Recently, a superheating phenomenon was found in epitaxial films on (RE)BCO/substrate (substrate = MgO, $LaAlO_3$ or $SrTiO_3$). The film can endure a higher temperature than the corresponding single crystal. Yan *et al*. reported that the Nd-123/MgO film has a superheating upper limit around 1098 ˚C [36]. Xu *et al.* claimed the YBCO buffered Nd-123/YBCO/MgO film can even endure temperatures

up to 1120 ˚C [37].

B. Artificial Pinning Centers, Microstructures and Superconducting Properties

The short coherence lengths and large anisotropies of the HTS materials generally lead to an intrinsic weak pinning of flux lines [39]. Such problem can be reduced by creating correlated defects, *e.g.*, columnar defects by irradiation [7], ion substitutions [38, 40, 41], and addition of second phases [42, 43]. As the weak pinning centers originate from the defects of crystals, an evolution method is to make artificial pinning sites by ionic substitutes. For (RE)BCO system, on the one hand, it is generally recognized that T_c strongly depends on the oxygen content, which directly affects the carrier concentration and $RE_{1+x}Ba_{2-x}Cu_3O_y$ solid solutions [21]. On the other hand, as shown in Figure 2(a), experiments show that Ba^{2+} site, CuO_2 planes and CuO chains can be substituted with other ions. Occasionally, this leads not only to increased pinning site densities, but also to an improvement of superconducting properties. For example, Ba-rich additions suppress $RE_{1+x}Ba_{2-x}Cu_3O_y$ solid solutions, which lead to improved J_c [44, 45]. Similar effect by dilute doping to the CuO_2 plane was found in zinc- or nickel-doped YBCO bulk [46, 47]. Subsequently, as shown in Figure 2(b), Ishii *et al.* [38] found that local disorder in CuO chains by dilute impurity doping is a more promising way to improve J_c than impurity doping in Ba sites or CuO_2 planes. Especially in RE^{3+} mixed binary, ternary and quaternary systems one can attain higher density of effective pinning centers by adjusting the ratio of RE elements [48, 49].

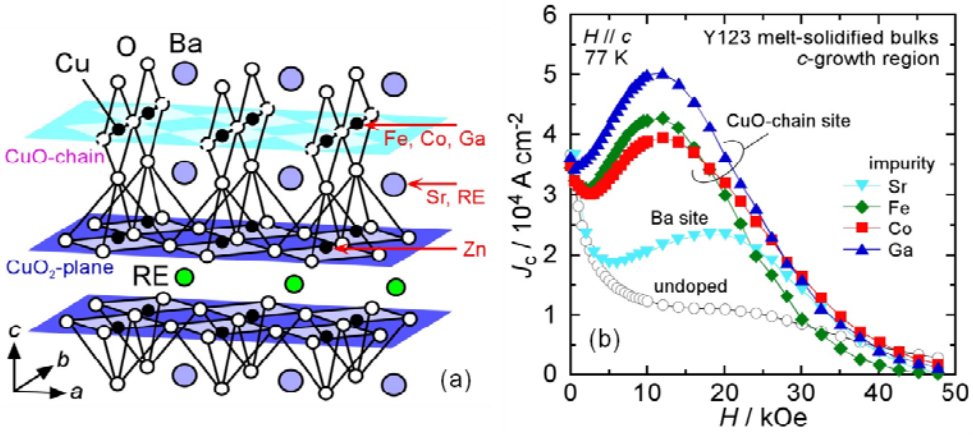

Fig. 2. (a) Illustration of the ionic substitutions. (J. Shimoyama, The University of Tokyo); (b) Comparison of J_c for various ion site substitutions [38].

According to the great compatibility of (RE)BCO system, many kinds of additions

are able to be incorporated in the matrix to act as pinning centers. It is well known that second phases of RE-211 or RE-422 enhance flux pinning. Among them, Gd-211 was found to produce the highest flux pinning. The T_p of Gd-123 is the lowest of all the (RE)BCO compounds. Thus, Gd-211 can nucleate at the lowest temperature, which is probably the reason for the typically small size of inclusions. The optimum content of Gd-211 is around 35 mol%.

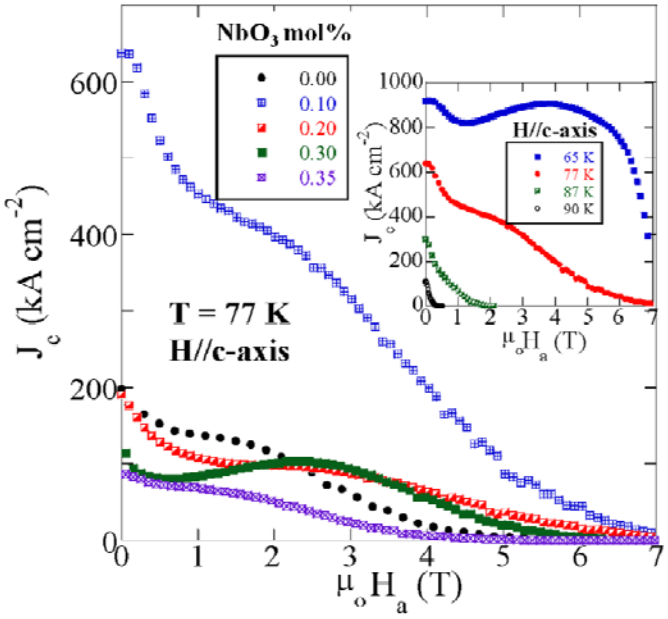

Fig. 3. J_c (B) curves for NEG-123 with 35 mol% fine Gd-211 (70nm), but various contents of NbO_3. Inset illustrates the J_c (B) curves at different temperature for the doping level of 0.1 mol% NbO_3 [50].

With nanometer sized Gd-211 (~ 70 nm) and NbO_3 particles (≤ 10 nm), Muralidhar *et al*. reported in the (Nd,Eu,Gd)BaCuO (NEG-123) system the prominent J_c values of 925 kA/cm^2 at 65 K, 640 kA/cm^2 at 77 K, and even 100 kA/cm^2 at 90 K, as shown in Figure 3 [50]. Similar result was also found with the addition of MoO_3 [50]. As shown in Figure 4, microstructure analysis indicates that there are three kinds of typical particles: NEG-211 or Gd-rich NEG-211 particles in size of 150 nm - 500 nm, $REBa_2CuZrO_y$ particles in size of 20 nm - 50 nm and Nb containing particles less than 10 nm. Note the initial average Gd-211 particle size is ~ 70 nm. Hence, the coarsening has happened.

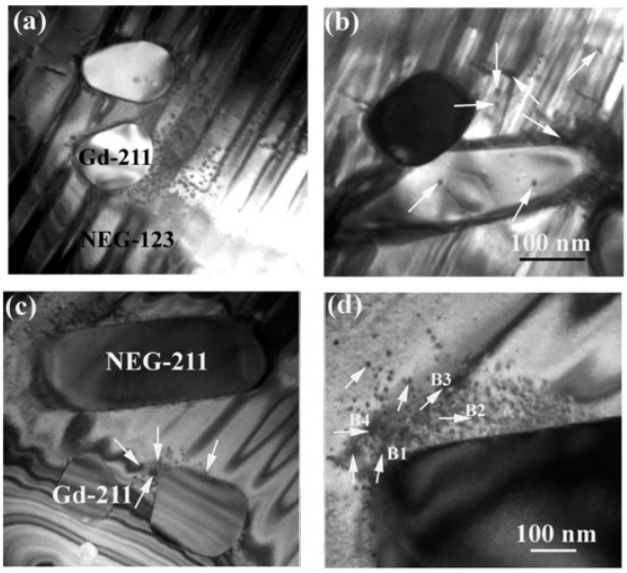

Fig. 4. TEM images of NEG-123 sample with 35 mol% Gd-211 (the initial average particle size is 70 nm) (a), and 0.1 mol% MoO_3 (b). The arrows point to some of the Mo based nano-sized particles < 10 nm. The (c) and (d) images are of NEG-123 sample with 0.1 mol% NbO_3. The arrows point to some of the Nb based nano-sized particles < 10 nm. [50]

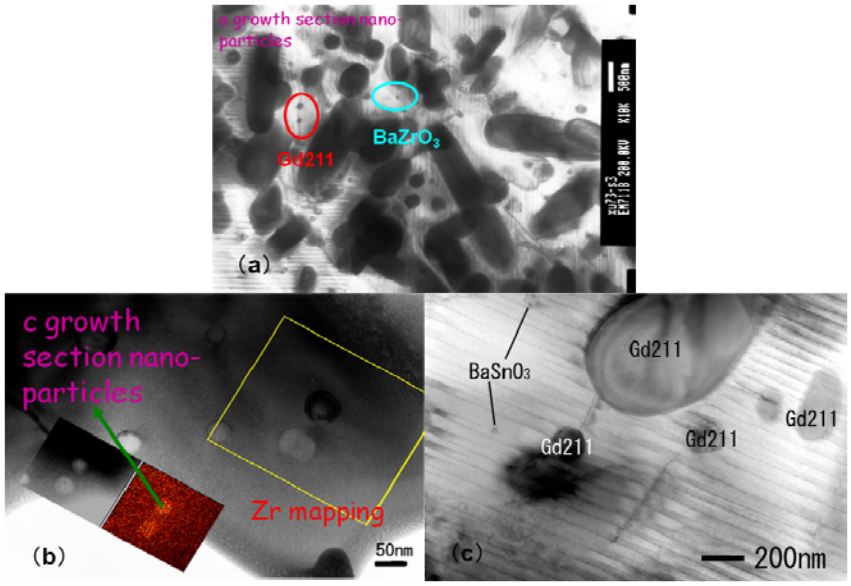

Fig. 5. TEM images of ZrO_2 and SnO_2 doped Gd-123 bulk: (a) shows a typical TEM image of ZrO_2 doped Gd-123 bulk. The typical nanometer-sized $BaZrO_3$ particle is indicated by blue circle. (b) A c-direction TEM image; insets illustrate the Zr element mapping. (c) A typical TEM image of SnO_2 doped Gd-123 bulk. The typical nanometer sized $BaSnO_3$ particles are indicated by black lines. [55]

Hari Babu *et al*. studied in the YBCO system other interesting second phases, namely $RE_2Ba_4CuMO_z$ (RE-2411, RE = Y, Sm or Gd, M = Nb, Ta, W, Mo, Zr, Hf, Ag, *etc*.) [15, 51-53]. They found Y-2411 large particles consist of agglomerated clusters of much smaller particles sized between 20 and 100 nm. Those nanometer particles can be dispersed by Ba-Cu-O liquid and retain their size during the melt growth. A typical size range of 20 to 50 nm was stably embedded in the YBCO matrix [52]. Hence, J_c has been improved remarkably by the combined Y-2411 with Y-211 [15, 52]. However, with different kinds of M ions, the properties of RE-2411 become different. Xu *et al.* found a band structure with the alternative distribution of Gd-211 and Gd-2411 (M = Mo) [54].

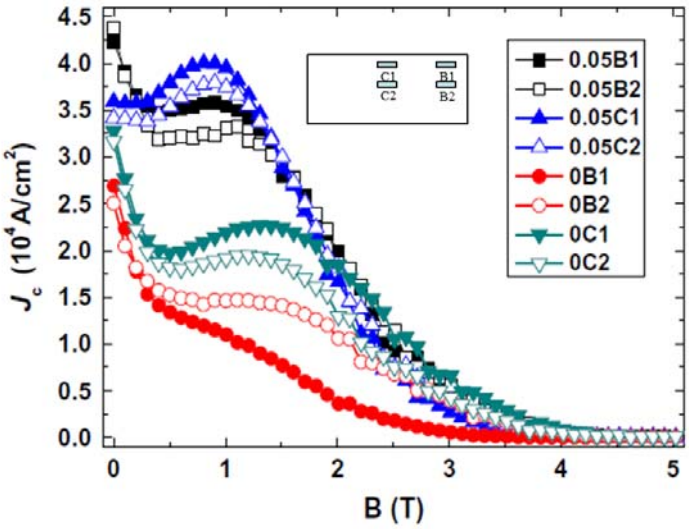

Fig. 6. J_c (B) curves at 77 K with B // c-axis of specimens which were cut from different parts of the standard bulk and 0.05 wt.% Fe-B alloy doped bulk. The inset illustrates the cut positions [56].

Pinning is optimized when the size of the defects approaches the coherence length and when the areal number density of defects is on the order of $(B/2) \times 10^{11}$ cm^{-2}, where B is the applied magnetic field in tesla [6, 17]. Such a high density has been difficult to achieve by material processing methods due to the coarsening of RE-211. Therefore, based on the second phase of RE-211, the addition of a small amount of foreign particles generally improves the pinning effect and J_c. Remarkable improvement of J_c has been achieved with the additions of 0.1 mol% NbO_3 as shown in Fig. 3. Experiment shows that Zr, Zn, Sn, Nb, Mo, Ti, Hf, Fe, Al are energetically favourable for flux

pinning with a dilute doping level range from 0.1 mol% to 1 mol%. To clarify the underlying nature of the enhancement in superconducting properties, systematic studies on the microstructure have been performed. Xu *et al*. [55] studied the microstructure of ZrO_2, SnO_2 and ZnO_2 doped Gd-123 bulks by using TEM, as shown in Figure 5. They found $BaZrO_3$ and $BaSnO_3$ particles in size of ~ 50nm formed in ZrO_2 and SnO_2 doped samples and contributed to the δl pinning[1] [56]. In contrast, doping of the bulk with ZnO_2 mainly contribute to the δT_c pinning[2] [56] due to the substitution of Cu sites by Zn. As a result, Zn-rich compounds were not observed.

As can be seen from Figure. 4 and Figure. 5, the presence of particles several tens of nanometer in size was always resulting in a particular supercurrent enhancement over a wide temperature range [50]. To date, the mechanism of collaborative flux pinning by the pinning structure with the particle size distribution ranging from microns to nanometers is not clear, but there is no doubt that those random distributed defects are very promising for practical applications.

Beside the single element doping, complex compound doping is also performed. Xu *et al*. [57,58] found that magnetic Fe-B alloy doping is able to enhance J_c, as shown in Fig 6, although T_c was suppressed significantly. Subsequently, Xu *et al*. reported [59] the Fe-B alloy particles to have decomposed while ferromagnetic Fe_3O_4 was formed. Tsuzuki *et al*. have compared the doping effect of Fe-B alloy and Fe_2O_3, and found Fe-B alloy doping is superior to Fe_2O_3 doping for the enhancement of pinning in Gd-123 bulk [60]. The issue of magnetic pinning is still under debate.

III. MAGNETIZATION TECHNIQUES

The trapped field of a bulk is not only determined by pinning centers, but also correlated with the magnetization process. Generally, four magnetization methods can be utilized: field-cooling (FC), zero-field cooling (ZFC), pulsed field magnetization (PFM) and flux pumping (FP). To trap the maximum possible field $B_{T,\,max}$, the required applied field B_A is, $B_A \geq B_{T,\,max}$ for FC, $B_A \geq 2\ B_{T,\,max}$ for ZFC, and $B_A \sim 4\ B_{T,\,max}$ or lower for pulsed ZFC. Using flux pumping full magnetization can be achieved with peak fields of $B_A \sim 0.25\ B_{T,\,max}$, by applying multiple cycles [19]. A variety of technical issues have been done for the aim of effective magnetization and flux trapping. For example, the PFM has been developed to generate the conical trapped field by

[1]The fBl pinning is caused by fluctuations of the charge carrier mean free path near a lattice defect.
[2]The fBT_c pinning is caused by spatial fluctuations of the transition temperature T_c.

Sugimoto *et al* [61] and further developed for rotating machinery applications [62].

IV. APPLICATIONS OF BULK (RE)BCO MATERIALS

Bulk (RE)BCO superconductors are potentially applied to three general categories in engineering, including levitation devices such as maglev, flywheels, seismic isolation, rotating machines as motors and generators, and trapped flux devices (sputtering systems, separators, drug delivery and nuclear magnetic resonance systems).

A. Magnetic Levitation

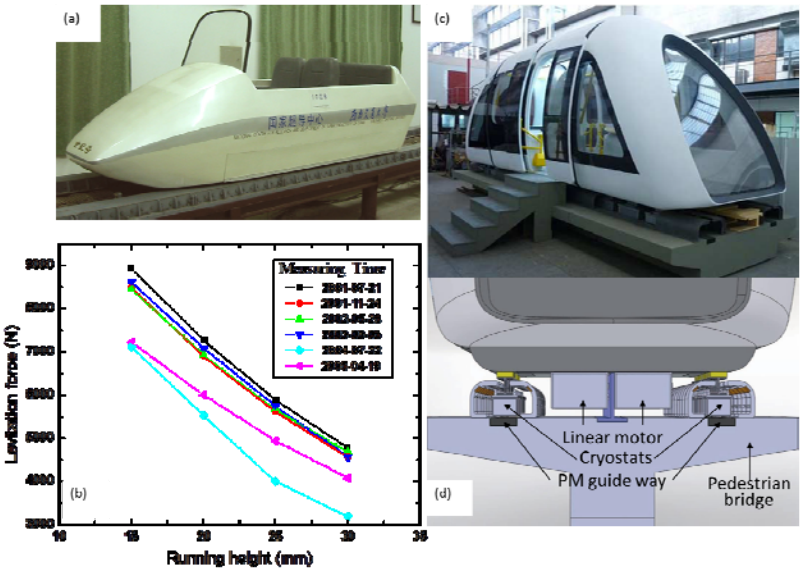

Fig. 7. (a) A photo of the first man-carrying HTS Maglev test vehicle (Southwest Jiaotong University, China). (b) Levitation force as a function of gap for different testing years [65]. (c) Design of a real-scale Maglev-Cobra four-sections vehicle [67]. (d) A schematic view of a part of propulsion and levitation of Maglev-Cobra on a pedestrian bridge [68].

As a potential ground rail transit tool of the future, HTS Maglev system has the unique property of passive self-stable levitation, in contrast to all the other Maglev technologies [63]. This property results in a variety of advantages, for example, low energy consumption, negligible noise emission, small track curvature radius (50 m), and capability to ascend ramps of 15 %.

In year 2000, the first man-carrying HTS Maglev vehicle demonstrations were

successfully completed in China [64]. The vehicle is shown in Figure 7(a). Using YBCO bulk magnets the vehicle has a levitation capability of 635 kg, and a lateral restoring force of 198 kg. Both the reliability and stability of this vehicle were demonstrated in longer-time operation, as shown in Figure 7(b) [65]. In the past decade, similar work have been carried out in Germany, Russia, Brazil, Japan, Italy and other countries [66]. Among these, a realistic vehicle called Maglev-Cobra stands out. Figure 7(c) show its external view (a photo) while Figure 7(d) is a somewhat schematic drawing of the vehicle on a pedestrian bridge [67, 68].

B. Flywheel

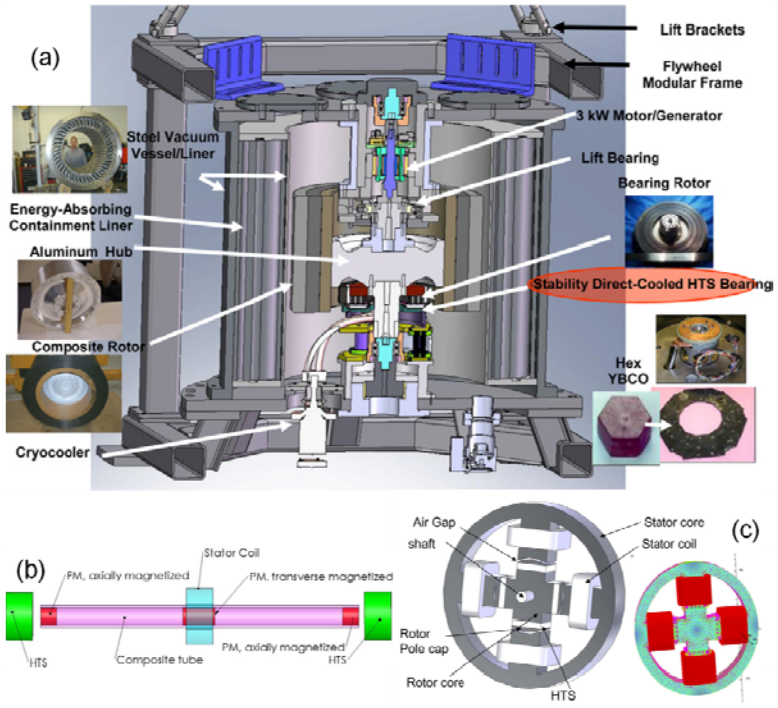

Fig. 8. (a) Overall design of the Boeing flywheel energy storage [69]. (b) Schematic of rotor components, HTS stators, and motor stator coils [70]. (c) The basic configuration of Boeing TF-HTS motor/generator [71].

HTS magnetic bearings offer extremely low rotational loss and make possible a high-efficiency flywheel diurnal energy storage. We present here only one example of a flywheel energy storage, that of Boeing, USA, shown in Figure 8 [69-71]. In 2007, Strasik *et al*. [72] have developed a 5 kWh/100 kW flywheel that rotates at 15, 000 rpm. So far, rotational speeds of 82,000 rpm in air and a 130, 400 rpm in vacuum have been achieved in Boeing. The future bearing speed goal is over 1,000,000 rpm.

C. Power Device Applications: Synchronous Motor

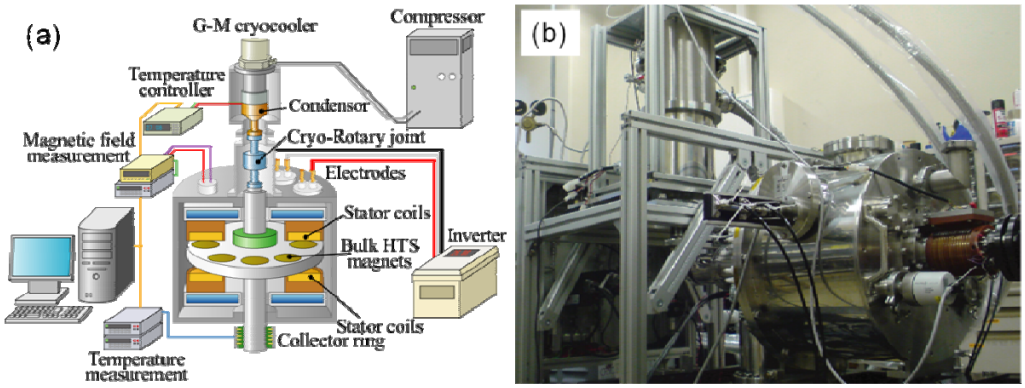

Fig. 9. (a) and (b) exhibit a schematic view of an axial-type of the bulk HTS synchronous motor and the peripheral systems and the constructed prototype system [73, 74].

The ability of bulk HTS to trap a large magnetic flux permits its use as a field pole on the motor. Initial experiments with bulk HTS motors have mostly shown that the entire motor can be situated in a liquid-nitrogen bath. We have reported a practical cryomechanical design in which the circulation of liquid nitrogen is restricted around the pole bulk HTS in the rotor plate [73,74]. In 2007, we have developed a complete closed-cycle thermosyphon (TS) cooling system using neon gas as cryogen. This TS successfully cooled down the bulk HTS parts below 40 K. We further improved the TS in 2009 and a two-phase (Ne-He) closed-cycle system is now in testing [73]. With the improved TS, the cooling of the eight Gd-123 bulk magnets comprised in the motor has been shortened from 2100 minutes to less than 400 minutes, for example, with a cooling power of about 50 W at 30 K. Figure 9(a) shows the schematic view of the bulk HTS synchronous motor with peripheral systems and Figure 9(b) is a photo of the constructed system. Recently, thanks to the bulk with an addition of magnetic Fe-B alloy particles and improvement of TS, we found the decay of the trapped flux of the Gd-123 field poles after 5 hours at 35 K synchronous operation was 7.2 % for a standard Gd-123 bulk without addition and 4.1 % for the Gd-123 with addition of Fe-B particles. The flux decay at 35 K is small and it was less than 50 % of the decay observed at 77 K [73, 74]. Thus, both the magnetic particle addition and lowering of the operating temperature suggest approaches to further development of propulsion motors and generators. In the next step, we have is to verify the limits of the maximum flux or torque that can be practically used in electric machines.

D. Magnetic Drug Delivery System (MDDS)

The MDDS is a technology to control the drug diffusion with the human body quantitatively, both spatially and temporally. It prevents the medicine from diffusing throughout the human body by selective transportation to the diseased part [75]. However, in the case of the accumulation of drug carrier ferromagnetic particles with small guiding permanent magnet, it is difficult to accumulate the particles even at short distances away from the magnet. Nishijima *et al*. [76] successfully made a MDDS by employing Gd-123 bulk as strong magnet to control the drug delivery. The probability of drug navigation to the desired direction was confirmed to be higher than 80 %.[3] They studied the appropriate diameter of liposome and the number of encapsulated ferromagnetic particles which can be controlled by the external magnetic force. Their result shows that the size of magnetite particles should > 100 nm to avoid macrophages. An optimal diameter of magnetite and liposome is 400 nm and 600 nm, respectively. After accumulation on the targeted part using magnetic force, the drug can be released from the liposome with an external stimulus (*e.g*., temperature) [77].

E. Magnetic resonance

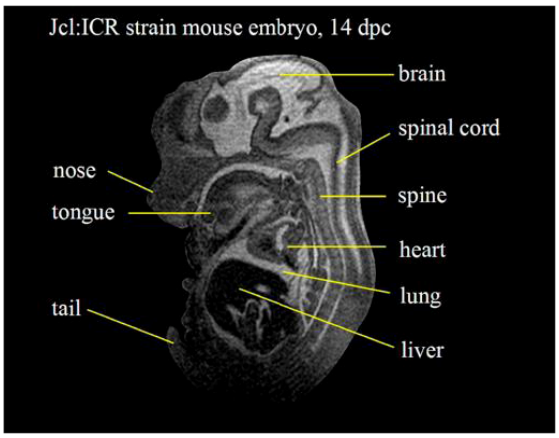

Fig. 10. A cross section of mouse embryo chemically fixed at 14 days post conception (dpc) measured using the MR microscope [79].

The HTS bulk magnet has also been used in nuclear magnetic resonance (NMR) and magnetic resonance imaging (MRI) due to the stable strong trapped flux and convenient cooling process. Nakamura *et al.* have studied a NMR system using Sm-123 bulk [78]. Magnetic resonance (MR) microscope is a magnetic resonance imaging (MRI) system

[3] The drug carrier, named liposome, was used to carry the ferromagnetic particles and the drug itself.

that achieves a spatial resolution of < 100 μm for small animals and intact specimens. Ogawa *et al*. studied the first MR microscope using a Eu-123 bulk. They have successfully achieved three-dimensional MR images of a chemically fixed mouse embryo acquired with voxels of $(50\ \mu m)^3$ [79]. Figure 10 shows a cross section of mouse embryo visualized by the microscope.

V. CONCLUSIONS

Recent progress on materials and their applications in the melt-growth (RE)BCO have been presented. A large scale bulk disk with a diameter up to 150 mm has been fabricated by employing the TSMG technique. To enhance the critical current density, the roles of different ion site substitutions were summarized. A significant J_c value of 640 kA/cm^2 under self-field at 77 K was achieved in the NEG-123 system with nanometer sized Gd-211 and transition-metal oxide particles. Microstructure analysis have indicated that the appearance of particles several tens of nanometers in size are always accompanied by a particular critical-current enhancement in a wide temperature range. By comparing the superconducting properties of the Gd123 bulk without and with addition of magnetic particles, we noticed enhancement of homogeneous pinning properties in the bulk with magnetic particles. This observation will guide us to towards the enhancement of the trapped flux. Several examples of HTS bulk devices on levitation and flux trapping described here prove that (RE)BCO bulks possess significant potential for high-field engineering applications due to high trapped field and compactness.

ACKNOWLEDGEMENTS

The present work was partially supported by KAKENHI (21360425), Grant-in-Aid for Scientific Research (B) and Grant-in-Aid for JSPS Fellows from Japan Society for the Promotion of Science (JSPS).

REFERENCES

[1] M.K. Wu, J.R. Ashburn, C.J. Torng, *et al*. *Phys. Rev. Lett.* **58**, 08 (1987).

[2] M. Tomita, M. Murakami, *Nature* **421**, 17 (2003).

[3] S. Nariki, N. Sakai, M. Murakami, *Supercond. Sci. Tech.* **18**, 126 (2005).

[4] A.M. Campbell, D.A. Cardwell, *Cryogenics* **37**, 67 (1997).

[5] A.P. Malozemoff, *Nat. Mater*. **6**, 17 (2007).

[6] D. Larbalestier, A. Gurevich, D.M. Feldmann, A. Polyanskii, *Nature* **414**, 368 (2001).

[7] L. Civale, A.D. Marwick, T.K. Worthington, *et al*., *Phys. Rev. Lett.* **67**, 648 (1991).

[8] T. Haugan, P.N. Barnes, R. Wheeler, *et al.*, *Nature* **430**, 867 (2004).

[9] X. Yao, Y. Shiohara, *Supercond. Sci. Tech.* **10**, 249 (1997).

[10] G. Desgardin, I. Monot, B. Raveau, *Supercond. Sci. Tech.* **12**, R115 (1999).

[11] R. Cloots, T. Koutzarova, J.P. Mathieu, M. Ausloos, *Supercond. Sci. Tech.* **18**, R9 (2005).

[12] P. Kazin, Y. Tretyakov, in: Y. Gogotsi (Ed.) *Nanomaterials Handbook*, CRC Press, (2006).

[13] C. Xu, A. Hu, N. Sakai, *et al.*, *Int. J. Condens. Matter. Adv. Mater. Supercond. Res.* **6**, 347 (2006).

[14] D.A. Cardwell, N.H. Babu, *Physica C* **445**, 1 (2006).

[15] N.H. Babu, Y.H. Shi, S.K. Pathak, *et al*., *Physica C,* **471**, 169 (2011).

[16] M. Muralidhar, M. Tomita, M. Jirsa, A.M. Luiz (Ed.), *Superconductor*, InTech, p.203 (2010).

[17] T. Matsushita, *Supercond. Sci. Tech.* **13**, 730 (2000).

[18] T. Matsushita, *Flux Pinning in Superconductors*, Berlin Heidelberg, New York: Springer (2007).

[19] R. Weinstein, D. Parks, R.P. Sawh, K. Davey, *Supercond. Sci. Tech.* **23**, 115015 (2010).

[20] K. Salama, S. Sathyamurthy, *Appl. Supercond.* **4**, 547 (1996).

[21] M. Murakami, N. Sakai, T. Higuchi, S.I. Yoo, *Supercond. Sci. Tech.* **9**, 1015 (1996).

[22] N. Sakai, S. Nariki, K. Nagashima, M. Miryala, *et al*., *Physica C* **460**, 305 (2007).

[23] S. Nariki, N. Sakai, M. Kita, *et al*., *Supercond. Sci. Tech.* **19**, S500 (2006).

[24] N. Sakai, K. Inoue, S. Nariki, A. Hu, M. Murakami, I. Hirabayashi, *Physica C* **426-431**, Part 1, 515 (2005).

[25] E.S. Reddy, T. Rajasekharan, *J. Mater. Res.* **13**, 2472 (1998).

[26] E.S. Reddy, T. Rajasekharan, *Supercond. Sci. Tech.* **11**, 523 (1998).

[27] E.S. Reddy, G.J. Schmitz, *Supercond. Sci. Tech.* **15**, L21 (2002).

[28] E.S. Reddy, J.G. Noudem, M. Tarka, G.J. Schmitz, *Supercond. Sci. Tech.* **13**, 716 (2000).

[29] E.S. Reddy, G.J. Schmitz, *Supercond. Sci. Tech.* **15**, 727 (2002).

[30] S. Meslin, K. Iida, N.H. Babu, *et al*., *Supercond. Sci. Tech.* **19**, 711 (2006).

[31] K. Iida, N.H. Babu, Y. Shi, D.A. Cardwell, *Supercond. Sci. Tech.* **18**, 1421 (2005).

[32] S. Meslin, J.G. Noudem, *Supercond. Sci. Tech.* **17**, 1324 (2004).

[33] N.D. Kumar, T. Rajasekharan, K. Muraleedharan, *et al*., *Supercond. Sci. Tech.* **23**, 105020 (2010).

[34] H.T. Ren, L. Xiao, Y.L. Jiao, M.H. Zheng, *Physica C* **412-414**, Part 1, 597 (2004).

[35] Y. Shi, N.H. Babu, D.A. Cardwell, *Supercond. Sci. Tech.* **18**, L13 (2005).

[36] S.B. Yan, L.J. Sun, T.Y. Li, *et al*., *Supercond. Sci. Tech.* **24**, 075007 (2011).

[37] H. H. Xu, Y. Y. Chen, L. Cheng, *et a*l., http://arxiv.org, (2011).

[38] Y. Ishii, J. Shimoyama, Y. Tazaki, *Appl. Phys. Lett.* **89**, 202514 (2006).

[39] P. Yang, C.M. Lieber, *Science* **273**, 1836 (1996).

[40] A. Das, M.R. Koblischka, N. Sakai, *et al.*, *Supercond. Sci. Tech.* **11**, 1283 (1998).

[41] M. Muralidhar, H.S. Chauhan, T. Saitoh, *et al.*, *Supercond. Sci. Tech.* **10**, 663 (1997).

[42] M. Murakami, H. Fujimoto, S. Gotoh, *et al*., *Physica C* **185-189**, 321 (1991).

[43] M. Muralidhar, T. Saitoh, K. Segawa, M. Murakami, *Appl. Supercond.* **4**, 535 (1996).

[44] C.X. Xu, A.M. Hu, N. Sakai, *et al*., *J. Supercond. Nov. Magn*. **20**, 309 (2007).

[45] C.X. Xu, A.M. Hu, N. Sakai, M. Izumi, I. Hirabayashi, *Supercond. Sci. Tech.* **18**, 229 (2005).

[46] G. Krabbes, G. Fuchs, P. Schätzle, *et al*., *Physica C* **330**, 181 (2000).

[47] L. Shlyk, G. Krabbes, G. Fuchs, *et al.*, *Supercond. Sci. Tech.* **18**, S10 (2005).

[48] M. Muralidhar, M. Jirsa, N. Sakai, M. Murakami, *Appl. Phys. Lett.* **79**, 3107 (2001).

[49] M. Muralidhar, S. Nariki, M. Jirsa, *et al*., *Appl. Phys. Lett.* **80**, 1016 (2002).

[50] M. Muralidhar, N. Sakai, M. Jirsa, *et al*, *Appl. Phys. Lett.* **92**, 162512 (2008).

[51] N.H. Babu, M. Kambara, Y. Shi, *et al*., *Physica C* **392-396**, Part 1, 110 (2003).

[52] N.H. Babu, K. Iida, Y. Shi, *et al*., *Supercond. Sci. Tech.* **19**, S461 (2006).

[53] N.H. Babu, K. Iida, L.S. Matthews, *et al*., *Mater Sci Eng. B-Adv*. **151**, 21 (2008).

[54] C.X. Xu, A.M. Hu, N. Sakai, *et al*., *Supercond. Sci. Tech.* **18**, 1082 (2005).

[55] C. Xu, A. Hu, M. Ichihara, *et al*., *Jpn. J. Appl. Phys*. **48**, 023002 (2009).

[56] G. Blatter, M. V. Feigel'man, V. B. Geshkenbein, *et al*., *Rev. Mod. Phys.* **66**, 1125 (1994).

[57] Y. Xu , K. Tsuzuki, S. Hara *et al.*, *Physica C* **470** 1219 (2010).

[58] Y. Xu, M. Izumi, K. Tsuzuki, *et al*., *Supercond. Sci. Tech.* **22**, 095009 (2009).

[59] K. Xu, K. Tsuzuki, S. Hara, *et al*., *Supercond. Sci. Tech.* **24**, 085001 (2011).

[60] K. Tsuzuki, S. Hara, Y. Xu, *et al*., *IEEE Trans. Appl. Supercon.* **21**, 2714 (2011).

[61] H. Sugimoto, T. Ida, M.Izumi *et al*., *Trans. Materials Research Society of Jpn*., **29**, 1311 (2004).

[62] E. Morita, H. Matsuzaki, Y. Kimura *et al*., *Supercond. Sci. Tech.* **19**, 1259 (2006).

[63] J. Wang, S. Wang, J. Zheng, *IEEE Trans. Appl. Supercond.* **19**, 2142 (2009).

[64] J. Wang, S. Wang, Y. Zeng, *et al*., *Physica C* **378-381**, Part 1, 809 (2002).

[65] J. Zheng, Z.G Deng, L.L. Wang, *et al*., *IEEE Trans. Appl. Supercond.* **17**, 2103 (2007).

[66] J. Wang, S. Wang, J. Zheng, *et al*., *IEEE Trans. Appl. Supercond.* **21**, 1551 (2011).

[67] G.G. Sotelo, D.H.N. Dias, R. de Andrade Jr., R.M.Stephan, *IEEE Trans. Appl. Supercond.* **21**, 1464 (2011).

[68] G.G. Sotelo, D.H.N. Dias, O.J. Machado, *et al*., *J. Phys.: Conf. Ser*. **234**, 032054 (2010).

[69] M. Strasik, J.R. Hull, J.A. Mittleider, *et al*., *Supercond. Sci. Tech.* **23**, 034021 (2010).

[70] J.R. Hull, M. Strasik, J.A. Mittleider, *et al*., *IEEE Trans. Appl. Supercond.* **19**, 2078 (2009).

[71] J.R. Hull, M. Strasik, *Supercond. Sci. Tech.* **23**, 124005 (2010).

[72] M. Strasik, P.E. Johnson, A.C. Day, *et al*., *IEEE Trans. Appl. Supercond.* **17**, 2133 (2007).

[73] B. Felder, M. Miki, Z. Deng, *et a*l., *IEEE Trans. Appl. Supercond.* **21**, 2213 (2011).

[74] M. Miki, B. Felder, K. Tsuzuki, *et al*., *IEEE T. Appl. Supercon.* **21**, 1185 (2011).

[75] Y. Hirota, F. Mishima, Y. Akiyama, S. Nishijima, *IEEE Trans. Appl. Supercond.* **20**, 826 (2010).

[76] S. Nishijima, S. Takeda, F. Mishima, *et al*., *IEEE Trans. Appl. Supercond.* **18**, 874 (2008).

[77] K. Nakagawa, F. Mishima, Y. Akiyama, S. Nishijima, *IEEE Trans. Appl. Supercond.* **21,** 3JP1-10 (2011).

[78] T. Nakamura, Y. Itoh, M. Yoshikawa, *et al*., *Concepts in Magnetic Resonance Part B: Magn. Reson. Eng.* **31B**, 65 (2007).

[79] K. Ogawa, T. Nakamura, Y. Terada, *et al*., *Appl. Phys. Lett.* **98**, 234101 (2011).